

DISCOVERY OF CH AND OH IN THE -513 km s^{-1} EJECTA OF η CARINAE

E. VERNER,^{1,2,3} F. BRUHWEILER,^{1,2} K. E. NIELSEN,^{1,2} T. R. GULL,¹ G. VIEIRA KOBER,^{1,4} AND M. CORCORAN⁵

Received 2004 September 16; accepted 2005 May 16

ABSTRACT

The very massive star η Carinae (η Car) is enshrouded in an unusual complex of stellar ejecta, which is highly depleted in C and O and enriched in He and N. This circumstellar gas gives rise to distinct absorption components corresponding to at least 20 different velocities along the line of sight. The velocity component at -513 km s^{-1} exhibits very low ionization with predominantly neutral species of iron-peak elements. Our statistical equilibrium/photoionization modeling indicates that the low temperature ($T = 760 \text{ K}$) and high density ($n_{\text{H}} \sim 10^7 \text{ cm}^{-3}$) of the -513 km s^{-1} component is conducive to molecule formation including those with the elements C and O. Examination of echelle spectra obtained with the Space Telescope Imaging Spectrograph (STIS) on board the *Hubble Space Telescope* (*HST*) confirms the model's predictions. The molecules H_2 , CH, and most likely OH have been identified in the -513 km s^{-1} absorption spectrum. This paper presents the analysis of the *HST* STIS spectra with the deduced column densities for CH, OH, and C I and an upper limit for CO. It is quite extraordinary to see molecular species in a cool environment at such a high velocity. The sharp molecular and ionic absorptions in this extensively CNO-processed material offer us a unique environment for studying the chemistry, dust formation processes, and nucleosynthesis in the ejected layers of a highly evolved massive star.

Subject headings: circumstellar matter — ISM: molecules — stars: individual (η Carinae) — ultraviolet: stars

1. INTRODUCTION

Eta Carinae is a luminous blue variable (LBV) of extremely high mass ($M_* \sim 100 M_{\odot}$) in a late phase of its evolution. Most of the nebulosity enshrouding η Car is a product of earlier ejection events. The bipolar structure, known as the Homunculus, was created during the great eruption in the 1840s, while a similar structure, the Little Homunculus (Ishibashi et al. 2003), resulted from a less significant eruption in the 1890s. Eta Car has undergone extensive mass loss and has a current mass-loss rate of $\dot{M} \sim 10^{-3} M_{\odot} \text{ yr}^{-1}$ (Hillier et al. 2001).

The stellar photosphere, as well as nebulosities both close to η Car and beyond the Homunculus, indicate significant CNO processing (Hillier et al. 2001). Emission-line spectra of the Weigelt blobs B and D, stellar ejecta at distances of ~ 200 – 600 AU , indicate extensive CNO processing (Verner et al. 2005). Even at much larger distances, optical/UV emission spectra show N enhancement within the soft X-ray-emitting shell surrounding η Car (Davidson et al. 1986; Smith & Morse 2004).

Observations using *HST* STIS of the central emission core containing the stellar source of η Car reveal a complex of narrow circumstellar absorption lines representing at least 20 distinct velocity components in the line of sight toward η Car. The high-velocity component at -513 km s^{-1} arises in a region of low temperature, $T = 760 \text{ K}$ (Gull et al. 2005). This resolved component is typified by both neutral and singly ionized elements.

A curve-of-growth analysis provided level populations and an excitation temperature, which were incorporated into statistical equilibrium/photoionization modeling similar to that used in Verner et al. (2002). Modeling of this cool component yielded a characteristic distance to the central star of $\log(R/\text{cm}) \sim 17.4$ for a density of $\log(n_{\text{H}}/\text{cm}^{-3}) \sim 7$. Another result of the modeling was the prediction of observable molecules in this fast-moving filament.

This paper presents the observationally derived column densities for CH and OH and upper limits for other relevant molecular and atomic species in the -513 km s^{-1} component. Examination of high-resolution *HST* STIS Multianode Microchannel Array (MAMA) spectra acquired with the E230H grating reveals definite detections of six absorption lines from CH and two probable OH line detections in the wavelength region between 3070 and 3150 Å. In addition, data at shorter wavelengths yield column densities for atomic C I and a column density upper limit for CO. Then, comparisons between modeling and observed column densities set further constraints on the physical conditions for the -513 km s^{-1} component. Over 800 H_2 Lyman absorption lines have been identified in the -513 km s^{-1} velocity component and are discussed elsewhere (Nielsen et al. 2005).

The observed Ti II, C I, and CH column densities serve as a basis for photoionization modeling that leads to predictions for other molecules in the high-velocity ejecta. These results require carbon and oxygen deficiencies, in agreement with CNO processing, to explain the observed molecules. Due to large uncertainties in defining parameters in the models, we can only estimate the possible range of physical conditions that are responsible for molecule formation.

2. OBSERVATIONS

The data for this paper were obtained as a part of several η Car *HST* programs using the high spatial and spectral resolution capabilities of STIS. The STIS observations were obtained with the E140M (1150–1730 Å) and the E230H (2885–3160 Å) gratings, providing a spectral resolving power of $R = 45,800$ and 114,000,

¹ Exploration of the Universe Division, Code 667, NASA Goddard Space Flight Center, Greenbelt, MD 20771; kverner@fe2.gsfc.nasa.gov, fredb@iacs.gsfc.nasa.gov, nielsen@stis.gsfc.nasa.gov, theodore.r.gull@nasa.gov, gvieira@stis.gsfc.nasa.gov.

² Institute for Astrophysics and Computational Sciences, Department of Physics, Catholic University of America, Washington, DC 20064.

³ Department of Engineering, Architecture, and Aerospace Technology, University of the District of Columbia, Washington, DC 20008.

⁴ Science Systems and Applications, Inc., Lanham, MD 20706.

⁵ Universities Space Research Association, 7501 Forbes Boulevard, Suite 206, Seabrook, MD 20706; and Exploring the Universe Division, NASA Goddard Space Flight Center, Greenbelt, MD 20771; corcoran@barnegat.gsfc.nasa.gov.

TABLE 1
DATA USED FOR THE η CAR -513 km s^{-1} EJECTA ANALYSIS

<i>HST</i> GO Program	Observing Date	JD - 2,450,000	Grating	Spectral Coverage (\AA)	Analyzed Species
9083.....	2002 Jan 20	2294.735	E140M	1150–1729	H ₂ , C I, CO
9083.....	2002 Jan 20	2294.831	E230H	2886–3158	OH, CH
9973.....	2003 Sep 21	2904.012	E230H	2378–3158	OH, CH

NOTE.—The central wavelengths for the E140M and the E230H gratings are 1425 and 3012 \AA , respectively.

respectively. Additional information about these observations is presented in Table 1.

3. MOLECULAR AND NEUTRAL ATOMIC SPECIES IN THE -513 km s^{-1} COMPONENT

3.1. CH and OH

The molecule CH is definitely present in the circumstellar environment of η Car. Figure 1 shows a portion of the E230H spectrum with identified CH lines at -513 km s^{-1} . Table 2 presents both measured values and upper limits for equivalent widths for CH transitions of the $C^2\Sigma^+-X^2\Pi$ system identified in the spectrum. Table 2 also includes observed and laboratory wavelengths for each CH transition, as well as the measured velocity, lower energy level of the transition, and gf -values from Kurucz (2004). We have searched for CH absorption lines from levels with an excitation energy up to 579 cm^{-1} above the ground state, but no detectable absorption is found from any levels with energies above 18 cm^{-1} , with a $\sim 2 \text{ m\AA}$ detection limit for the individual lines. The reader is referred to Figure 2 of Lien (1984) for the term structure of CH including Λ doubling. The absence of absorption from energy levels higher than 18 cm^{-1} implies a very low excitation temperature for CH, $T \leq 30 \text{ K}$. This is significantly below the 760 K inferred from the level populations for Ti II (Gull et al. 2005).

For all derived column densities, we assume that the features lie on the linear curve of growth. Comparisons with the curve of growth for a b -value of 2.1 km s^{-1} , derived for the -513 km s^{-1} component from the Ti II lines, indicate that this assumption is reasonable. The average velocity of the observed CH lines is $-513.2 \pm 1.7 \text{ km s}^{-1}$, which is in good agreement with the corresponding value derived from the Ti II lines. Based on the results (Table 2), the total CH column density is $N_{\text{CH}} = 5.4 \times 10^{13} \text{ cm}^{-2}$.

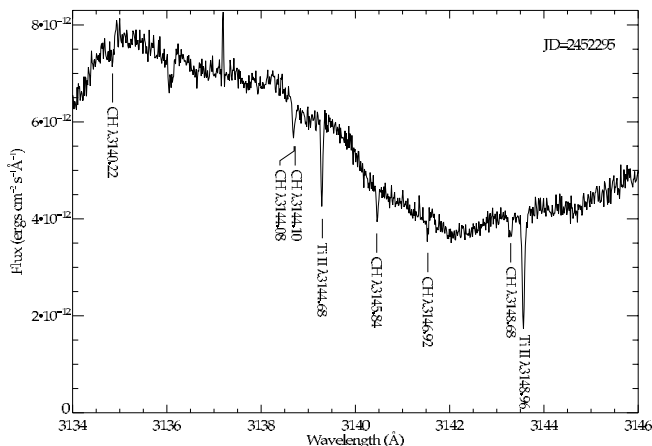


FIG. 1.—Spectrum in the 3134–3146 \AA range obtained with the *HST* STIS in 2002 January (JD = 2,452,295). The positions of six CH and two strong Ti II lines are marked by solid lines and their laboratory wavelengths.

Although such studies are beyond the scope of this paper, we further note that the CH lines in the -513 km s^{-1} component show temporal variability between 2002 January and 2003 September. We have used only the 2002 January data to derive column densities.

Two weak OH lines, $\lambda\lambda 3079, 3082$, are identified in the -513 km s^{-1} absorption spectrum (Figs. 2 and 3) and presented in Table 3. To confirm the presence of these spectral features, a spectrum obtained in 2003 September has been used for comparison. Line identification of the OH features was accomplished using molecular data presented in Roueff (1996). No weaker OH transitions are observed. Based on the equivalent widths of the OH $\lambda\lambda 3079, 3082$ features, 1.9 ± 1.0 and $2.3 \pm 1.0 \text{ m\AA}$, respectively, we adopt an OH column density of $N_{\text{OH}} = (3 \pm 1) \times 10^{13} \text{ cm}^{-2}$. Given the weakness of these two lines, even though there is a good velocity correlation, we consider OH a probable detection in the circumstellar gas in the line of sight to η Car.

3.2. Atomic Carbon, C I

We have identified C I lines arising from all three fine-structure levels of the ground term in the -513 km s^{-1} component (see Fig. 4). Neither the presence of C I nor its excitation should be surprising, yet, the excitation of the fine-structure levels can lead to additional constraints on the physical conditions in this component. Because most of these C I transitions are blended and approaching saturation, we have derived approximate C I column densities based on weaker features that have resolved C I contributions. The results for specific lines from the differing fine-structure levels in the ground configuration are given in Table 4. C I, C I*, and C I** refer to transitions originating from the zero, 16.4, and 43.4 cm^{-1} levels, respectively. The E140M spectrum, in which the C I lines are present, has lower spectral resolution ($R = 45,800$) than the E230H one. We have used the

TABLE 2
IDENTIFIED CH LINES IN THE η CAR -513 km s^{-1} EJECTA

λ_{lab} (\AA)	J_l	E_l (cm^{-1})	$\log gf^a$	λ_{obs} (\AA)	Velocity (km s^{-1})	W_λ (m\AA)
3144.079.....	1/2	0.00	-2.28	3138.678	-515.0	6.3 ± 2.0^b
3144.102.....	1/2	0.00	-1.98	3138.722	-513.0	...
3146.922.....	1/2	0.04	-1.98	3141.525	-514.1	...
3145.836.....	3/2	17.77	-1.53	3140.459	-512.6	6.0 ± 2.0
3140.221.....	3/2	17.81	-1.93	3134.852	-512.6	...
3148.683.....	3/2	17.81	-1.70	3143.302	-512.3	7.0 ± 2.0
3145.071.....	3/2	66.84	-1.53	<2
3150.749.....	3/2	67.11	-1.71	<3
3145.679.....	5/2	73.07	-1.34	<2
3151.330.....	5/2	73.19	-1.55	<2.4

NOTES.—Values are based on 2002 January data, E230H. All transitions are from the $C^2\Sigma^+-X^2\Pi$ system, 0–0 band ($\sigma_0 = 31778 \text{ cm}^{-1}$).

^a Kurucz (2004).

^b Value is $\sum W_{\text{CH}}$ for CH $\lambda\lambda 3144.079, 3144.102$.

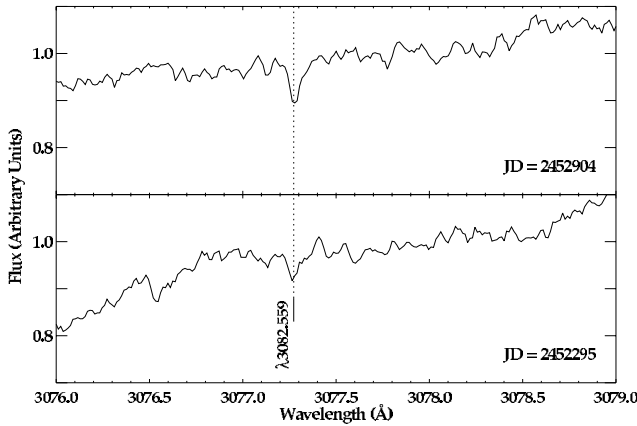


FIG. 2.—Spectra in the 3076–3079 Å range obtained with the *HST* STIS in 2002 January and 2003 September. The position of the OH line is marked by the dotted line and its laboratory wavelength in each spectrum.

best-resolved components of the transitions of C I to estimate column densities. Several lines appear to be unblended, with no discernible overlap with other transitions, namely, C I $\lambda\lambda$ 1328.833, 1657.379, 1658.121. By adopting a curve of growth corresponding to a $b = 2.1 \text{ km s}^{-1}$, as found for the Ti II (Gull et al. 2005), we derive $\log(N_{\text{C I}}/\text{cm}^{-2}) = 13.8$, $\log(N_{\text{C I}^*}/\text{cm}^{-2}) = 13.6$, and $\log(N_{\text{C I}^{**}}/\text{cm}^{-2}) = 14.0$. Here, we specifically bias the result based on the weaker C I lines, since the deduced column densities are less sensitive to saturation effects. The average velocities of these lines are $514.1 \pm 1.7 \text{ km s}^{-1}$. Summing these column densities gives a total C I column density of $N_{\text{C I}(\text{tot})} = 2 \times 10^{14} \text{ cm}^{-2}$.

We have further used the ratios $f_1 = N_{\text{C I}^*}/N_{\text{C I}(\text{tot})}$ and $f_2 = N_{\text{C I}^{**}}/N_{\text{C I}(\text{tot})}$ to estimate the pressure, $P/k = nT \text{ (cm}^{-3} \text{ K)}$ for the neutral carbon absorbing region (e.g., Jenkins 2002; Jenkins & Shaya 1979). The resulting $f_1 = 0.3$ and $f_2 = 0.5$ are close to their LTE values. With the uncertainties, we find that $\log[nT/(\text{cm}^{-3} \text{ K})] \geq 6$, given the temperature, 760 K, based on the analysis of the Ti II lines (Gull et al. 2005).

With the exception of H_2 , the most abundant molecular species in the interstellar medium (ISM) is typically CO. However, C and O may be depleted up to 100 times in the η Car environment (Dufour et al. 1997; Hillier et al. 2001; Verner et al. 2005). Negligible CO may be present in the ejecta. Nevertheless, we did search for CO. The CO features from the $A^1\Pi-X^1\Sigma^+$ bands (0–0 through 7–0) fall in the spectral range 1300–1520 Å. Based on f -values, the strongest band is the (0–0) band near 1510 Å, and

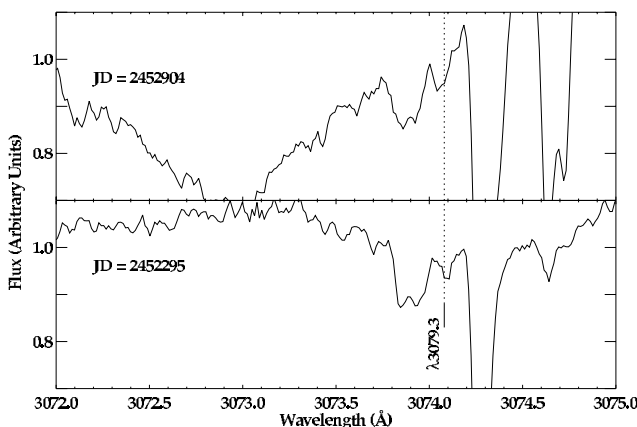


FIG. 3.—Spectra in the 3072–3075 Å range obtained with the *HST* STIS in 2002 January and 2003 September. The position of the OH line is marked by the dotted line and its laboratory wavelength in each spectrum.

TABLE 3
OH LINES IN THE η CAR -513 km s^{-1} EJECTA
FROM THE $A^2\Sigma^+-X^2\Pi_{3/2}$ SYSTEM, 0–0 BAND

λ_{lab} (Å)	J_l	E_l (cm^{-1})	$\log gf^a$	λ_{obs} (Å)	Velocity (km s^{-1})	W_λ (mÅ)
3082.559.....	3/2	0.00	-2.59	3077.262	-515.1	2.3 ± 1.0
3079.36 ^b	3/2	0.00	-2.38	3074.093	-512.8	1.9 ± 1.0

NOTE.—Values are based on 2002 January data, E230H.

^a Roueff (1996).

^b Width is $\sum W_{\text{CH}}$ for OH $\lambda\lambda$ 3079.36,3079.23; $\log gf$ -value reflects sum of both lines.

the bands get weaker toward shorter wavelengths. Using the CO data from Morton & Noreau (1994), we searched for the strongest lines in these bands at velocities within $\pm 5 \text{ km s}^{-1}$ of -513 km s^{-1} for each transition wavelength. In all cases, we have equivalent width upper limits of $W_\lambda \leq 3 \text{ mÅ}$ for the $R(0)$ lines of the (0–0) and (1–0) bands. Likewise, features from other, weaker bands yielded nondetections. Using the f -values for the $R(0)$ transition in the (0–0) band to impose an upper limit, we find that $\log(N_{\text{CO}}/\text{cm}^{-2}) \leq 12.95$. This upper limit could be slightly higher, depending upon how the rotational levels are populated. The CO upper limit is 5–6 times less than the derived column of CH and 3 times less than our possible detection of OH. This is in sharp contrast with what is found in the ISM, where in the case of the line of sight to ζ Oph and other stars, the CO is roughly 100 times more abundant than CH (cf. van Dishoeck & Black 1986).

3.3. Molecular Hydrogen, H_2

Molecular hydrogen has been observed in the -513 km s^{-1} ejecta (Smith 2002; Nielsen et al. 2005). As stated earlier, over 800 features arising from the Lyman bands have been identified. The absorption lines from the Lyman bands, as seen by *HST* STIS, are from high vibrational and rotational states. Ground-state transitions are inaccessible in the *HST* wavelength range. We have made a rough estimate of the H_2 column density based on the Lyman absorption in the -513 km s^{-1} component. For $T = 760 \text{ K}$, we estimate a lower limit to the H_2 column density to be $\sim 10^{16} \text{ cm}^{-2}$ based on H_2 Lyman absorption from higher

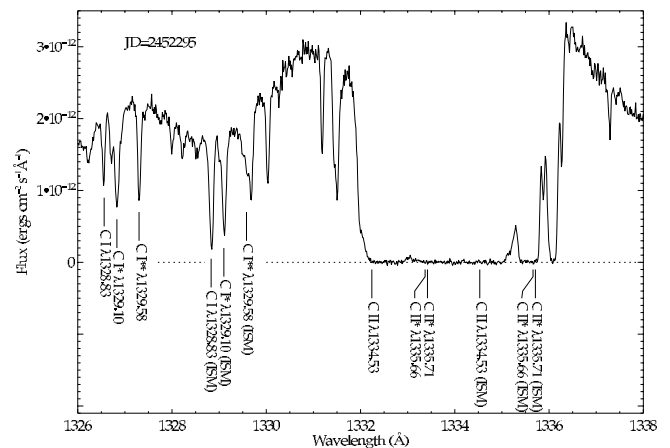


FIG. 4.—Spectrum in the 1326–1338 Å range obtained with *HST* STIS in 2002 January (JD = 2,452,295). The positions of the detected C I and possible C II lines are marked by solid lines and laboratory wavelengths. The expected presence of C II in the fast ejecta is completely obscured by the broad, saturated C II λ 1335 stellar wind profile in the same region. Positions of the C I and C II lines originated in the ISM are plotted for comparison.

TABLE 4
MEASURED C I LINES IN THE η CAR -513 km s^{-1} EJECTA

λ_{lab} (Å)	J_l	E_l (cm^{-1})	$\log gf^a$	W_λ (mÅ)	$N_{C\text{ I}}$ (cm^{-2})
1270.143.....	0	0.00	-3.41	<3	...
1280.135.....	0	0.00	-1.58	18.6:	...
1328.833.....	0	0.00	-1.34	29.8 ± 4	13.8
1560.309.....	0	0.00	-1.11	58.8:	...
1656.928.....	0	0.00	-0.83	54.4:	...
1329.578.....	1	16.40	-0.64	49.5:	...
1656.267.....	1	16.40	-0.73	48.3:	...
1657.379.....	1	16.40	-0.95	23.5 ± 4	13.6
1658.128.....	2	43.40	-0.73	38.7 ± 4	14.0
1661.438.....	2	43.40	-0.49	60.1:	...

^a Morton (2003).

energy states ($E > 11,000 \text{ cm}^{-1}$) and assuming Boltzmann statistics. However, the relative populations may be altered significantly from LTE conditions in several ways: (1) by radiative rates (Sternberg & Dalgarno 1989) and (2) by a contribution from an additional hidden cold ($T < 760 \text{ K}$) component. The excitation conditions for H_2 are beyond the scope of this paper and will be addressed elsewhere. A total column density for H_2 in the range of $\sim 10^{20} \text{ cm}^{-2}$ would not be unreasonable. In any event, any estimate of the H_2 total column density is highly uncertain.

4. PHYSICAL CONDITIONS IN THE EJECTA

Due to the complex circumstellar environment of η Car, it is difficult to develop a unique photoionization model describing the whole system. The most effective way is to model separately each velocity component to obtain the physical conditions in the gas. The binary system may contain a very luminous B star and a less luminous O or WN star, where the radiation field in the surrounding nebula can vary dramatically over the orbital phase (Verner et al. 2005). In many distinct ejecta the excitation conditions change over the 5.54 yr period (Damineli 1996; Corcoran et al. 2001). Because of the constant strength and low ionization of the atomic absorption in the -513 km s^{-1} component, we assume that the most important excitation and ionization source for ejecta at a large distance is the radiation field of the primary B star. Verner et al. (2002) found that a radiation field of $T_{\text{eff}} = 15,000 \text{ K}$ for the central star for the distance of the Weigelt B and D blobs reproduced the presence and strengths of strong Fe II and [Fe II] emission lines in these nebular condensations.

We have attempted to explain the origin of CH, CO, and OH molecules of high-velocity ejecta quantitatively. We have used the photoionization code CLOUDY, version 96 (Ferland et al. 2005). This recent version includes about 1000 reactions for ~ 70 molecules containing H, He, C, O, N, Si, and S with reaction rates taken from the UMIST database (Le Teuff et al. 2000). The general chemical formalism included in CLOUDY has been described in earlier works (e.g., Hollenbach & McKee 1979, 1989; Tielens & Hollenbach 1985a, 1985b; Lenzuni et al. 1991). Under low-temperature conditions, atomic H may be converted into H_2 (Hollenbach & McKee 1979). The associative detachment of H^- may efficiently produce H_2 in the high-velocity ejecta via the reaction $\text{H}^- + \text{H} \rightarrow \text{H}_2 + e^-$. Hollenbach & McKee (1979, 1989) also suggested that CH formation is possible via reactions (1) $\text{C} + \text{H}_2 \rightarrow \text{CH} + \text{H}$ or (2) $\text{C}^+ + \text{H}_2 + e^- \rightarrow \text{CH} + \text{H}$. Both processes could be effective in this dense component. The first route (1) only needs the high temperature to activate the

reaction. The second route (2) is a series of two or three reactions either at high temperature (form CH^+ , then form CH^{+2} , and then recombine) or having a small temperature dependence for radiative combination, which forms CH^{+2} directly.

To model the physical conditions in the -513 km s^{-1} component, we must specify the luminosity, the energy distribution in ionizing flux, the distance from central source to the ejecta, and the elemental abundances in the ejecta.

We have used a model atmosphere flux distribution (Kurucz 2003) corresponding to $T_{\text{eff}} = 15,000 \text{ K}$, as in our previous work (Verner et al. 2005). We have adopted the distance $\log(R/\text{cm}) = 17.4$ from the central stellar source to the -513 km s^{-1} absorption component (Gull et al. 2005). Independent studies of elemental abundances in stellar spectra (Hillier et al. 2001), Weigelt blobs (Dufour et al. 1997; Verner et al. 2005), and in the S condensation beyond the Homunculus (Davidson et al. 1986) demonstrated that He and N are enhanced by a factor of 5 and 10 compared to solar values, respectively. While we have adopted He and N abundances, the C and O abundances are not fixed in the models. Previous attempts to explain physical conditions by using a single-density model in a complex η Car environment led to the range for electron densities n_e from 10^5 to 10^{10} cm^{-3} (Hamann et al. 1999). This large uncertainty has resulted in the varied hydrogen density in the model from $\log(n_{\text{H}}/\text{cm}^{-3}) = 5.0$ to 9.0.

We have no constraints on how much dust is present in this ejecta. However, we expect that dust plays an important role in molecule formation in such a cold environment. Moreover, since carbon is highly depleted in η Car due to CNO processing, we expect that the grains are predominantly silicates. We have included Orion Nebula-like silicates in the calculations and varied the hydrogen density and amount of dust in the model to obtain the best fit with the observed column densities of $N_{\text{C I}(\text{tot})} = 2 \times 10^{14} \text{ cm}^{-2}$ (§ 3.2) and $N_{\text{Ti II}(\text{tot})} = 2 \times 10^{14} \text{ cm}^{-2}$ (Gull et al. 2005).

Due to uncertainties in the modeling, including properties and amount of dust, elemental abundances, thickness of the ejecta, and hydrogen density, we can only constrain an approximate range of parameters where CH and other molecules form. We have found that for the density range of $n_{\text{H}} \sim 10^6 - 10^{7.5} \text{ cm}^{-3}$, the required total amount of silicates is 2–10 times larger than that in the Orion Nebula. At a lower density, more dust is needed in the calculations to reproduce the observed CH column density. Another important constraint is the H_2 column density, where we only have a lower limit, as discussed previously.

To demonstrate the sensitivity of molecule formation to various parameters, we present four different representative models and information from observations in Table 5. For each model, Table 5 has the adopted values of C/H and O/H abundance relative to the solar value and shows whether or not it includes dust and X-ray flux. Table 5 also gives the calculated shell thickness (ΔR), given as $\log(\Delta R/\text{cm})$, as well as the average temperature (T_{ave}) and predicted logarithmic column densities of Ti II, C I, H_2 , CH, CO, OH, and other important molecules. All models adopt a constant density $n_{\text{H}} = 10^7 \text{ cm}^{-3}$, the distance $\log(R/\text{cm}) = 17.4$ from the central source to the ejecta, a He abundance 5 times the solar value, and a N abundance 10 times the solar value. Table 5 also includes the deduced values derived from the species Ti II, C I, H_2 , CH, CO, and OH and excitation temperatures derived from Ti II and CH. A portion of the ion-molecule chemistry that occurs in the cold molecular cloud may require a source providing ionization beyond 13.6 eV. In addition to UV radiation from the primary B star, η Car is known to be a variable in X-rays with a 5.54 yr period. The source of these X-rays is likely due to a binary wind-wind interaction (Corcoran et al. 2001). We have

TABLE 5
COMPARISON BETWEEN OBSERVATIONS AND MODELS
FOR THE η CAR -513 km s^{-1} EJECTA

PARAMETER	OBSERVATIONS	MODELS ^a			
		1	2	3	4
T_{ave} (K)	993	572	1120	1010
$T_{\text{Ti II}}$ (K)	760
T_{CH} (K)	30
$\log(\Delta R/\text{cm})$	14.8	14.8	14.4	14.8
C	0.1	0.1	1	0.01
O	0.01	0.01	1	0.01
X-ray	yes	no	yes	yes
Dust	yes	yes	no	yes
$\log(N_{\text{H}_2}/\text{cm}^{-2})$	> 16	20.7	20.7	13.7	20.7
$\log(N_{\text{C}_2}/\text{cm}^{-2})$	14.3	14.9	14.9	14.1	13.9
$\log(N_{\text{Ti II}}/\text{cm}^{-2})$	14.3	14.8	14.8	14.5	14.8
$\log(N_{\text{CH}}/\text{cm}^{-2})$	13.7	13.2	13.2	6.7	12.3
$\log(N_{\text{OH}}/\text{cm}^{-2})$	13.5	13.8	13.7	10.4	13.8
$\log(N_{\text{CO}}/\text{cm}^{-2})$	≤ 12.95	12.7	12.6	8.3	11.8
$\log(N_{\text{CH}^+}/\text{cm}^{-2})$	12.2	12.3	10.1	11.3
$\log(N_{\text{CH}_2}/\text{cm}^{-2})$	12.5	12.6	...	11.6
$\log(N_{\text{NH}}/\text{cm}^{-2})$	11.9	11.3	9.0	11.8
$\log(N_{\text{NH}_3}/\text{cm}^{-2})$	8.2	5.6	...	8.2

^a All models are calculated at $\log(R/\text{cm}) = 17.4$ and $\log(n_{\text{H}}/\text{cm}^{-3}) = 7$. The thickness of the cloud, ΔR , is in cm, and the column densities are listed. The C and O abundances are presented relative to solar values. The X-ray flux is based on *Chandra* observations (M. Corcoran et al. 2005, in preparation). Dust assumes the Orion silicates dust with an amount 2.5 times larger than that in the Orion Nebula. We have indicated whether the dust or and X-rays are included in the model by “yes” and “no.” See the text for more details. Predictions on other molecules are available upon request from kverner@fe2.gsfc.nasa.gov.

included an X-ray continuum in the 0.054–1 keV band of $10^{37.9} \text{ ergs s}^{-1}$, which is consistent with the recent identification of He II $\lambda 4686$ (Steiner & Damiani 2004) and also consistent with the unabsorbed soft X-ray flux seen in a *Chandra* spectrum of η Car taken on 2003 May 3 (M. Corcoran et al. 2005, in preparation).

In our representative models, the amount of silicates is fixed at 2.5 times that in the Orion Nebula (dust to gas ratio [by mass]: ~ 0.004). In part due to the presence of both grains and X-ray flux, the local grain-gas photoelectric heating rate reached $>80\%$ of the total. Models 1 and 2 provide the best fit to observations (Table 5). The C abundance is 0.1 of the solar value, and the O abundance is 0.01 of the solar value. They both contain grain physics (van Hoof et al. 2004), but model 2 lacks an X-ray contribution. Comparison between model 1 and model 2 shows the effects of X-ray heating by the increased average temperature, T_{ave} . However, there are no significant differences in observable column densities. The only possible discriminant might be the NH column density.

To illustrate effects of different physical processes, models 2 and 3 are calculated. Model 3 has solar C and O elemental abundances with no dust, but includes X-ray flux. The comparison of model 3 and model 1 demonstrates the key role of dust for H_2 , CH, and CO formation. The predicted molecular column densities without dust are substantially below that observed. The presence of dust provides both a site for molecular formation and a source of pronounced extinction at wavelengths in the far-UV.

Model 4 in Table 5 demonstrates the effects of C and O depletion. This model is essentially the same as model 1, except for different C and O abundances. In this model, we have adopted C and O abundances derived from analysis of the Weigelt blobs B and D (Verner et al. 2005), where both C and O indicate abun-

dances of 0.01–0.02 times the solar value. In this model, the amounts of O and C are set at 0.01 of the solar value. The only observed molecule containing O is OH. Its predicted column density exhibits no apparent dependence on C abundance. The only observed molecule containing C is CH. As expected, the differences between models 1 and 4 indicate that the CH column density scales with the C abundance. While the O abundance is found to be the same for the Weigelt blobs and for the ejecta, C appears to be enhanced 5–10 times relative to the blobs (but 0.1 of the solar value) in the -513 km s^{-1} component. If these results reflect true abundance differences, one possible explanation could be inhomogeneous mixing of CNO-processed material with surrounding, less synthesized material in the nebula surrounding η Car.

Although models 1 and 2 provide a basic overall agreement with the observed column densities or constraints, there are still several unresolved problems. The elemental gas abundances in these calculations, except for CNO, are assumed to be solar. Specifically, no allowances for depletion onto dust grains are included. If allowances were made, the Ti/C abundance ratio would be lower, assuming that the abundances would follow the trends expected from condensation temperatures (cf. Lodders 2003). If we were to adopt a depletion of 0.6 dex, which is that of Si in the diffuse ISM (Gnaniński 2003), an element with a condensation temperature close to that for Ti, the agreement with observations would be good. Still, the predictions for C I, although acceptable, are not good. Since C I has an ionization potential of 11.26 eV, the amount of C I is extremely sensitive to both the amount of dust and the shape of the extinction curve in the far-UV. This sensitivity makes the C I predictions somewhat uncertain. This uncertainty also affects the molecular species containing carbon. The huge difference in observationally derived temperatures of CH lines ($T \leq 30 \text{ K}$) and Ti II lines ($T = 760 \text{ K}$) suggests that there must be temperature and/or density variations within the filament comprising the -513 km s^{-1} component. Large temperature differentials between metal and molecules are known in photodissociation regions (PDRs; Storzner and Hollenbach 1999). Absorptions of CH and Ti II arising in such different temperature regimes cannot be explained by a single-density photoionization model. We speculate that dusty clumps within the filament may provide an inhomogeneous temperature structure within the filament. These dusty clumps would provide an efficient way to spatially differentiate the Ti II and CH regions.

In a CNO-processed gas with subsolar C and O, molecules with N should be noticeably enhanced. Table 5 shows predicted NH and NH_3 column densities, which are smaller than those of CH, OH, and CO. Observations of these molecules would be quite important in verifying the N-rich molecular formation scenario. Two possibilities include observations of NH in absorption and NH_3 in emission. No spectral lines of NH are located in the region covered by the *HST* STIS MAMA (1140–3160 Å). The strongest NH line accessible at optical and UV wavelengths is the $R_1(0)$ line of the $A^3\Pi-X^3\Sigma^-(0-0)$ band at 3358.053 Å. However, this line is quite weak and normally requires very high resolution and signal-to-noise ratio to detect. For example, in ζ Oph it has an equivalent width of $\sim 0.4 \text{ mÅ}$ (Crawford & Williams 1997). Yet, an enhanced N abundance could improve the chances of detection. Observations of emission from the rotational transitions of NH_3 in the 23.7–24.1 GHz region offer a much better possibility (cf. Rizzo et al. 2001; Caproni et al. 2000).

In addition to predicting molecular lines in the ejecta, the photoionization modeling suggests the presence of the following strong lines in the IR: [C I] $1.069 \mu\text{m}$, [O I] $63.17 \mu\text{m}$, [Si II]

34.81 μm , [P II] 136.57 μm , and [Cl I] 14.34 μm . These lines should be investigated in future high spatial resolution observations for improved understanding of the excitation conditions, chemical abundances, and dust physics.

5. CONCLUSIONS

The *HST* STIS spectra of the absorption lines produced in the CNO-processed stellar ejecta around η Car show the definite presence of molecular species in the -513 km s^{-1} velocity component. The main conclusions are as follows.

1. The molecules H_2 and CH are positively identified, while OH is most likely present in the absorption spectrum. All of these features have velocities within $\pm 2 \text{ km s}^{-1}$ of the previously measured Ti II -513 km s^{-1} component. The column densities of observed species are given in the Table 5.

2. The nondetection of CO in the UV is consistent with the inferred low C and O abundances, as found in previous studies. The referee points out that “any PDR code, even with the C and O abundances adopted, would give both CH and OH columns greater than CO. OH tends to react quickly to form CO, in cases where C is greater than O in gas-phase abundance” and also that “it is easy to get more CH than CO if the C abundance is greater than O, but the hard part is to then get more OH than CO.”

3. Using our previous density constraint, $6.0 \leq \log(n_{\text{H}}/\text{cm}^{-3}) \leq 7.5$, for the -513 km s^{-1} component (Gull et al. 2005), we can produce CH column densities that are comparable to that in observations. However, based on our qualitative modeling, we cannot rule out the possibility that the CH is formed at higher densities.

4. The inadequacies in the modeling can partially be explained by the differences in implied temperatures, as seen in the

Ti II and CH with excitation temperatures of 760 K and less than 30 K, respectively. The -513 km s^{-1} component may well be inhomogeneous along the line of sight.

5. The modeling is not in complete agreement with observations. These differences might be explained by temporal variability, inhomogeneities in temperature and density, or a still-incomplete description for chemistry and dust. These problems can only be resolved by improved modeling and observations revealing other molecular species, providing additional constraints.

The presence of molecules in the ejecta of η Car and our modeling indicates that other molecular species, such as CH^+ , CH_2^+ , CH_2 , NH_3 , and NH , may be detectable, both via absorption and emission at other wavelengths. The unusually high densities of the gas and the apparent N-rich environment of the ejecta offer a unique opportunity to probe the nitrogen-based chemistry in the circumstellar regions of a highly evolved massive star.

We thank the anonymous referee for useful comments that improved the paper. The research of E. V. has been supported through an NSF grant (NSF-0206150) to the Catholic University of America. The investigators, T. R. G., E. V., K. E. N., and G. V., have been supported through the *HST* STIS GTO and GO programs. This paper is based on observations made with the NASA/ESA *Hubble Space Telescope*, obtained at the Space Telescope Science Institute, which is operated by the Association of Universities for Research in Astronomy, Inc., under NASA contract NAS 5-26555. *HST* GO program 9973 was part of the η Car Treasury Program, K. Davidson Principal Investigator.

REFERENCES

- Caproni, A., Abraham, Z., & Vilas-Boas, J. W. S. 2000, *A&A*, 361, 685
 Corcoran, M., Ishibashi, K., Swank, J. H., & Petre, R. 2001, *ApJ*, 547, 1034
 Crawford, I. A., & Williams, D. A. 1997, *MNRAS*, 291, L53
 Damineli, A. 1996, *ApJ*, 460, L49
 Davidson, K., Dufour, R., Walborn, N., & Gull, T. 1986, *ApJ*, 305, 867
 Dufour, R., Glover, T. W., Hester, J. J., Curie, D. G., van Orsow, D., & Walter, D. K. 1997, in *ASP Conf. Ser. 120, Luminous Blue Variables: Massive Stars in Transition*, ed. A. Nota & H. Lamers (San Francisco: ASP), 255
 Ferland, G. J., Abel, N., Davidson, K., & Smith, N. 2005, in *ASP Conf. Ser. 332, The Fate of the Most Massive Stars*, ed. R. Humphreys & K. Stanek (San Francisco: ASP), 298
 Gnacinski, P. 2003, *Acta Astron.*, 53, 379
 Gull, T. R., Vieira, G., Bruhweiler, F., Nielsen, K. E., Verner, E., & Danks, A. 2005, *ApJ*, 620, 442
 Hamann, F., Davidson, K., Ishibashi, K., & Gull, T. 1999, in *ASP Conf. Ser. 179, Eta Carinae At The Millennium*, ed. J. A. Morse, R. M. Humphreys, & A. Damineli (San Francisco: ASP), 116
 Hillier, D. J., Davidson, K., Ishibashi, K., & Gull, T. R. 2001, *ApJ*, 553, 837
 Hollenbach, D., & McKee, C. F. 1979, *ApJS*, 41, 555
 ———. 1989, *ApJ*, 342, 306
 Ishibashi, K., et al. 2003, *AJ*, 125, 3222
 Jenkins, E. B. 2002, *ApJ*, 580, 938
 Jenkins, E. B., & Shaya, E. J. 1979, *ApJ*, 231, 55
 Kurucz, R. L. 2003, CD-ROM 18, *Synthesis Programs and Line Data* (Cambridge: SAO)
 Kurucz, R. L. 2004, *Database for Molecules* (Cambridge: SAO), <http://kurucz.harvard.edu/LINELISTS>
 Lenzuni, P., Chernoff, D. F., & Salpeter, E. E. 1991, *ApJS*, 76, 759
 Le Teuff, Y. H., Millar, T. J., & Markwick, A. J. 2000, *A&AS*, 146, 157
 Lien, D. J. 1984, *ApJ*, 284, 578
 Lodders, K. 2003, *ApJ*, 591, 1220
 Morton, D. C. 2003, *ApJS*, 149, 205
 Morton, D. C., & Noreau, L. 1994, *ApJS*, 95, 301
 Nielsen, K. E., Gull, T. R., & Vieira Kober, G. 2005, *ApJS*, 157, 138
 Rizzo, J. R., Martin, P., Pintado, J., & Henkel, C. 2001, *ApJ*, 553, L181
 Roueff, E. 1996, *MNRAS*, 279, L37
 Smith, N. 2002, *MNRAS*, 337, 1252
 Smith, N., & Morse, J. 2004, *ApJ*, 605, 854
 Steiner, J. A., & Damineli, A. 2004, *ApJ*, 612, L133
 Sternberg, A., & Dalgarno, A. 1989, *ApJ*, 338, 197
 Storz, H., & Hollenbach, D. 1999, *ApJ*, 515, 669
 Tielens, A. G. G. M., & Hollenbach, D. 1985a, *ApJ*, 291, 722
 ———. 1985b, *ApJ*, 291, 747
 van Dishoeck, E. F., & Black, J. H. 1986, *ApJS*, 62, 109
 van Hoof, P., Weingartner, J. C., Martin, P. G., Volk, K., & Ferland, G. J. 2004, *MNRAS*, 350, 1330
 Verner, E., Bruhweiler, F., & Gull, T. R. 2005, *ApJ*, 624, 973
 Verner, E., Gull, T. R., Bruhweiler, F., Johansson, S., Ishibashi, K., & Davidson, K. 2002, *ApJ*, 581, 1154